Available online at www.sciencedirect.com
SCIENCE DIRECT®
Journal of Colloid and Interface Science 271 (2004) 1–15
JOURNAL OF Colloid and Interface Science
www.elsevier.com/locate/jcis

EXAFS study of mercury(II) sorption to Fe- and Al-(hydr)oxides I. Effects of pH ☆

Christopher S. Kim,[a,*] James J. Rytuba,[b] and Gordon E. Brown Jr. [a,c]

[a] *Surface and Aqueous Geochemistry Group, Department of Geological and Environmental Sciences, Stanford University, Stanford, CA 94305-2115, USA*
[b] *U.S. Geological Survey, 345 Middlefield Road, MS 901, Menlo Park, CA 94025, USA*
[c] *Stanford Synchrotron Radiation Laboratory, SLAC, 2575 Sand Hill Rd., MS 99, Menlo Park, CA 94025, USA*

Received 16 September 2002; accepted 21 March 2003

Abstract

The study of mercury sorption products in model systems using appropriate in situ molecular-scale probes can provide detailed information on the modes of sorption at mineral/water interfaces. Such studies are essential for assessing the influence of sorption processes on the transport of Hg in contaminated natural systems. Macroscopic uptake of Hg(II) on goethite (α-FeOOH), γ-alumina (γ-Al_2O_3), and bayerite (β-$Al(OH)_3$) as a function of pH has been combined with Hg L_{III}-edge EXAFS spectroscopy, FTIR spectroscopy, and bond valence analysis of possible sorption products to provide this type of information. Macroscopic uptake measurements show that Hg(II) sorbs strongly to fine-grained powders of synthetic goethite (Hg sorption density $\Gamma = 0.39$–0.42 μmol/m^2) and bayerite ($\Gamma = 0.39$–0.44 μmol/m^2), while sorbing more weakly to γ-alumina ($\Gamma = 0.04$–0.13 μmol/m^2). EXAFS spectroscopy on the sorption samples shows that the dominant mode of Hg sorption on these phases is as monodentate and bidentate inner-sphere complexes. The mode of Hg(II) sorption to goethite was similar over the pH range 4.3–7.4, as were those of Hg(II) sorption to bayerite over the pH range 5.1–7.9. Conversion of the γ-Al_2O_3 sorbent to a bayerite-like phase in addition to the apparent reduction of Hg(II) to Hg(I), possibly by photoreduction during EXAFS data collection, resulted in enhanced Hg uptake from pH 5.2–7.8 and changes in the modes of sorption that correlate with the formation of the bayerite-like phase. Bond valence calculations are consistent with the sorption modes proposed from EXAFS analysis. EXAFS analysis of Hg(II) sorption products on a natural Fe oxyhydroxide precipitate and Al/Si-bearing flocculent material showed sorption products and modes of surface attachment similar to those for the model substrates, indicating that the model substrates are useful surrogates for the natural sediments.

Keywords: EXAFS; Mercury; Sorption; Goethite; γ-Alumina; Bayerite; Bond valence

1. Introduction

The transport of mercury in aqueous environments is directly influenced by sorption to particle surfaces. Hg can become associated with streambed sediments, suspended particles, precipitated matter, natural organic matter, and other substrates that can settle out and effectively remove Hg from the mobile aqueous phase. This is particularly true in remote lake regions where atmospherically deposited Hg(II) and Hg(0) are the primary sources of Hg contamination [1–3] or at industrial sites that have released elevated concentrations of Hg in waste effluents [4,5]. In these areas, dissolved Hg represents a significant proportion of the Hg present, and the uptake of Hg onto particles is one of the dominant mechanisms that leads to its sequestration in sediments.

Hg uptake on particle surfaces also occurs in Hg-mineralized areas where extensive mining of Hg ore has resulted in large volumes of abandoned Hg-bearing mine tailing piles and in gold-mining regions where Hg was introduced for gold amalgamation. Although speciation analyses have shown that the Hg in these mine wastes is present primarily as Hg mineral phases such as cinnabar (HgS, hexagonal) and metacinnabar (HgS, cubic) [6,7], some of the minor phases identified (e.g., Hg chlorides, oxides and oxychlorides and elemental Hg(0)) are sufficiently soluble under ambient conditions to be leached from the piles through surface and rainwater infiltration. Dissolved Hg released from the tailings, although representing a minor proportion of the total Hg in these enriched regions, has a disproportionately higher degree of environmental significance with respect to

☆ Part II was published in J. Colloid Interface Sci. 270 (2004) 9–20.

* Corresponding author.
E-mail address: chriskim@pangea.stanford.edu (C.S. Kim).

0021-9797/$ – see front matter
doi:10.1016/S0021-9797(03)00330-8

potential bioavailability, toxicity, and human health. Therefore, sorption of Hg onto particles, whether the Hg source is atmospheric, industrial, or anthropogenic via mining, is an important process controlling its mobility in the aqueous environment.

The aqueous speciation and coordination of Hg have been well documented. The oxidation states of Hg in aqueous systems are 0, +1, and +2 [8]; in typical aerated waters, however, Hg(II) is most stable [9]. For this reason, the majority of Hg uptake studies have focused on Hg(II) compared to the more reduced oxidation states. Aqueous Hg(II) speciation and coordination in the absence of other strongly complexing ligands is largely dictated by hydrolysis reactions. At low pH, the hexaqua ion $Hg(H_2O)_6^{2+}$ is octahedrally coordinated by water molecules, with Hg–O bond lengths of 2.34–2.41 Å [10,11]. As the pH is raised and the extent of hydrolysis increases to $HgOH^+$ and $Hg(OH)_2$, two of the Hg–O bonds are shortened to distances of 2.00–2.10 Å, while the remaining bonds are lengthened to about 2.50 Å [10–13]. The distorted octahedral coordination that results, featuring two close axial oxygens and four more distant equatorial oxygens, gives the appearance of 2-coordinated Hg. This relatively unique coordination chemistry in water is indicative of the tendency for Hg(II) to form mononuclear linear 2-coordinated complexes, as also occurs in halides (HgI_2, $HgBr_2$), oxoanions ($(HgSO_3)_2^{2-}$, $Hg(NO_3)_2$), and certain solids ($HgCl_2$, HgO) [14]. It also explains the stability of the $Hg(OH)_2$ complex in the pH range of natural waters (5–9) as demonstrated in Fig. 1.

Studies of Hg(II) sorption have been conducted on numerous natural and synthetic substrates, including clays [15–19], metal oxides and sulfides [20–26], soils [27–34], and coals or activated carbon [35,36]. Of these potential sorbents, Fe and Al (hydr)oxides are particularly abundant in natural aquatic systems such as lakes and rivers and are effective substrates for Hg sorption. The majority of Hg sorption studies have relied upon macroscopic uptake measurements, which generally observe pH-dependent uptake of Hg(II) onto the substrates, consistent with cation sorption theory [37] and with the formation of the $Hg(OH)_2$ aqueous species through hydrolysis. Relatively fewer investigations (e.g., [35,38–40]) have used spectroscopic methods to study the Hg(II) sorption processes occurring at particle surfaces on a molecular scale. A detailed understanding of these specific reactions is essential for defining the mode(s) of Hg(II) sorption and the stability of the Hg sorption products, both of which have implications for its potential remobilization and bioavailability. Additionally, it is important to determine the dependence of these sorption modes on geochemical variables common to natural aquatic systems such as pH, complexing ligands, dissolved organic carbon (DOC), and ionic strength.

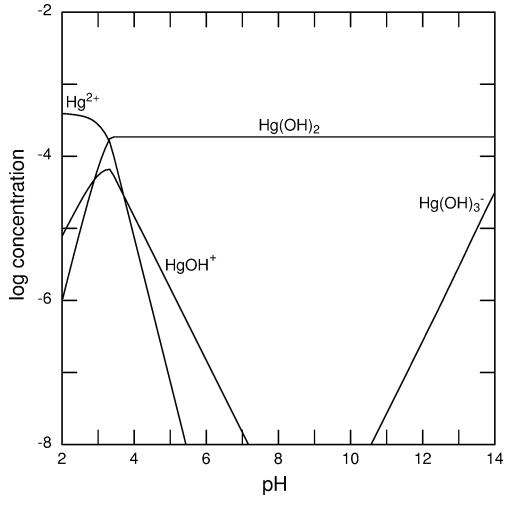

Fig. 1. Aqueous speciation diagram of Hg(II) (initial concentration = 0.5 mM) as a function of pH. Stability constants from Baes and Mesmer [9] were used in constructing the diagram.

Extended X-ray absorption fine structure (EXAFS) spectroscopy is uniquely suited for studying sorption reactions of heavy metal cations, as it can directly determine the local molecular structure around a metal ion in a sorbed state. More specifically, EXAFS spectroscopy can provide detailed information such as identity and number of nearest neighbor and second neighbor atoms around a central Hg atom, interatomic distances between Hg and these neighboring atoms, and degree of structural order, all of which are needed to characterize the mode(s) of Hg(II) sorption onto a specific surface. Additionally, EXAFS spectroscopy is nondestructive and samples can be run in situ (i.e., with water present) and require minimal preparation, allowing the analysis of samples under ambient conditions representative of complex natural environments.

The bond valence theory developed by Pauling in 1929 [41] has been utilized extensively in the analysis of crystalline [42–44] and amorphous materials [45,46] and has more recently been applied by Bargar et al. [47–49], Hiemstra, van Riemsdijk, and co-workers [50,51], and Ostergren et al. [52] to adsorbed metal complexes at the mineral/water interface. The correlation between bond length and bond strength (s, or valence) for a given bond, combined with the bond valence constraint of Pauling's second rule ($\sum s_{\mathrm{M-O}} \sim |\text{formal charge of ion}|$), provides a computationally simple method for predicting the coordinative stability of specific sorption complexes at a surface. As such, bond valence analyses can serve as a useful complement to EXAFS analysis of sorption complexes at mineral/water interfaces by placing basic bonding constraints on possible vs unlikely modes of sorption for a particular sorption system.

The objectives of this study, the first in a two-part series, are to use EXAFS spectroscopy to characterize the modes of Hg(II) sorption to goethite (α-FeOOH), γ-alumina (γ-Al_2O_3), and bayerite (β-$Al(OH)_3$) and to investigate how total Hg(II) uptake and sorption modes may be impacted as a function of pH. The second part of this study [53] examines the effects of chloride and sulfate, two complexing ligands that are commonly found in natural aquatic environments, on the macroscopic uptake and mode of Hg(II) sorption onto

the same three substrates. For both studies, synthetic, well-characterized materials are used for model system sorption experiments. In the current study, uptake of Hg(II) onto natural fine-grained precipitate samples is also conducted for comparison and to determine the relevance of the model substrates used. The bond valence approach is also applied to assess the coordinative stability of the sorption complexes proposed from the EXAFS data.

2. Experimental methods

Goethite was prepared by base (NaOH) titration of a ferric nitrate solution followed by equilibration at 60 °C and dialysis as described by Atkinson et al. [54]. The γ-alumina and bayerite were purchased from Degussa (CAS No. 1344-28-1) and Condea (Pural BT, Lot 15144), respectively. A Beckman–Coulter SA3100 surface area analyzer was used to measure the surface areas of the substrates using the BET method [55]. Goethite, γ-alumina, and bayerite were determined to have surface areas of 91, 97, and 9 m^2/g, respectively. High-surface-area materials were desired in order to assure sufficient Hg(II) uptake for EXAFS analysis. XRD and TEM analysis confirmed each substrate to be well crystallized, free from detectable impurities, and of relatively uniform particle size. Measured particle sizes and morphologies were as follows: goethite was present as 200×30 nm acicular crystals, γ-alumina as 10- to 20-nm spherical particles, and bayerite as 140×90 nm tabular crystals.

Two natural fine-grained substrates were also used in single-uptake experiments (i.e., pH dependency was not explored): an Fe-(hydr)oxide precipitate collected from the Knoxville mercury mine (Knoxville district, CA) and an Al/Si-bearing flocculent precipitate from Clear Lake, adjacent to the Sulphur Bank mercury mine (Clear Lake district, CA) [56]. Both materials formed downstream from their respective mining sites as a product of acid mine drainage and are essentially X-ray amorphous, although each displays XRD peaks indicating the presence of minor amounts of quartz. The two sorbents have measured BET surface areas of 195 and 33 m^2/g, respectively.

Batch uptake experiments were conducted in an aqueous 0.1 M $NaNO_3$ solution with N_2 gas bubbling through the sample vessels (50-ml Nalgene centrifuge tubes) throughout the course of the experiments to remove CO_2 and other gases. A mass of 0.5 g of solid was suspended in a final volume of 50 ml, resulting in a solids concentration of 10 g/l. A series of γ-alumina sorption samples was also prepared using 0.25 g of solid in order to minimize the amount of bayerite formed due to hydration of γ-alumina. For all uptake experiments, the pH was titrated down to 4 using 20-µl aliquots of 0.1 M HNO_3 before 5 ml of a 5 mM $Hg(NO_3)_2$ Mallinckrodt stock solution preserved in nitric acid (Lot 4737) was added to achieve a final solution concentration of 0.5 mM Hg(II) (100 ppm Hg), driving the pH level down to around 3.2. Such high concentrations of Hg(II) were necessary to ensure sufficient Hg(II) uptake onto the substrates for adequate EXAFS analysis. While the experimental Hg(II) concentration greatly exceeds those in natural systems, it is not expected to significantly alter the method of uptake since the concentration is too low to induce surface precipitation. Using 20-µl aliquots of 0.1 M NaOH, the pH was titrated back up to the desired level before the total volume was brought up to 50 ml. Samples were capped and equilibrated on a rotator for a minimum of 24 h before EXAFS analysis.

Following equilibration, samples were centrifuged at 15,000 rpm for 15 min and the supernatants separated from the solids. The final pH levels of the supernatants were measured prior to filtration with a 0.45-µm filter and acidification to pH$<$2 using concentrated HNO_3. All supernatants were analyzed for Hg(II) using a TJA IRIS Advantage/1000 Radial inductively coupled plasma (ICP) spectrometer. The extent of Hg(II) uptake onto the solids was calculated assuming no significant loss to the sample vessel walls (as verified through control samples).

To confirm the formation of bayerite suspected during the γ-alumina uptake experiments, an experiment was conducted to isolate and characterize the secondary phase that formed when γ-alumina reacted with the aqueous solution. A γ-alumina suspension was prepared by suspending 0.5 g of solid in 50 ml of 0.1 M $NaNO_3$ and titrating to pH 4 using 20-µl aliquots of 0.1 M HNO_3. The suspension was then centrifuged at 15,000 rpm for 15 min and the supernatant filtered with a 0.2-µm filter. This filtration step effectively separated the substrate from the solution following equilibration with the γ-alumina at pH 4, as verified by passing a He–Ne laser beam through the solution to confirm the removal of γ-alumina particles (no light scattering was detected). At this point, 5 ml of 5 mM $Hg(NO_3)_2$ was added to the filtered supernatant to achieve 0.5 mM Hg(II) and the pH brought back up to 6 with 20-µl aliquots of 0.1 M NaOH. Light scattering from the laser was observed during the titration to pH 6, indicating the formation of a secondary Al precipitate. This precipitate was later identified by FTIR analysis as a bayerite-like phase. The solution was filtered through a 2.5-µm filter using a Millipore filtration system and the filter paper was collected for EXAFS analysis.

Sorption products were loaded as moist pastes into sample holders and analyzed using EXAFS spectroscopy. In the case of the γ-alumina precipitation experiment, EXAFS data were collected directly off the damp filter paper. All EXAFS data were collected at the Stanford Synchrotron Radiation Laboratory (SSRL) on wiggler-magnet beamline 4–3 using Si(111) or Si(220) monochromator crystals. Hg L_{III}-edge EXAFS spectra were collected on the sorption samples at room temperature in the fluorescence-yield mode using a 13-element, high-throughput germanium detector. This method is optimized for low-concentration samples [57] and enabled collection of high-quality Hg L_{III}-EXAFS spectra from the sorption products generated. Ar-

senic and aluminum filters served to attenuate elastic scattering and background matrix fluorescence, respectively. EXAFS data were processed using the EXAFSPAK data analysis software package [58]. Phase and amplitude functions for quantitative fitting of the background-subtracted spectra were generated from model structures using FEFF 7.0 [59].

EXAFS spectra were fit by (i) isolating and fitting the first-shell Fourier transform feature to provide starting values for coordination number (CN), interatomic bond distance (R), and energy shift (E_0); (ii) isolating and fitting the second and/or more distant Fourier transform features using the E_0 value derived from the first-shell fitting; and (iii) fitting the complete background-subtracted, k^3-weighted EXAFS spectra using the CN, R, and E_0 values from the filtered fitting steps as the initial values of these variables. The scale factor (S_0) was fixed at 0.9 for all samples, based on previous experience in fitting well-characterized crystalline model compounds in which the scale factor was allowed to vary during fitting. The Debye–Waller factor (σ^2), which serves as a measure of thermal vibration and static disorder around Hg in the sample, was set at values appropriate to those of sorption complexes (0.005 for first-shell atomic neighbors, 0.01 for second- and third-shell neighbors) based on experience with other sorption systems. The molecular modeling programs Cerius^2 and Spartan Pro were used to generate visual representations of the various Hg sorption complexes proposed from interpretation of EXAFS fitting results. Energy minimization and structural optimization features of these two programs were employed to determine realistic interatomic distances and structural arrangements of the proposed Hg sorption complexes.

Diffuse reflectance infrared Fourier transform (DRIFT) spectroscopy of selected samples was conducted on a Nicolet Nexus 470 FT-IR spectrometer equipped with a DRIFT cell. Samples were run as air-dried powders, with pure unreacted γ-alumina and bayerite serving as the model endmembers for characterization of the Hg(II)-γ-alumina sorption samples. The Hg oxidation state of the initial $Hg(NO_3)_2$ stock solution was confirmed by Raman microscopy using a HoloLab Series 3000 Raman microscope from Kaiser Optical Systems, Inc. based on the identification of stretching frequencies consistent with $HgNO_3^+$ and $Hg(NO_3)_2$ [60,61] and the absence of Hg–Hg stretching frequencies common to Hg(I) aqueous species and solid compounds [62,63].

Bond valence analysis was conducted using the bond length and bond valence ranges for Fe–O, Al–O, Hg–O, and H–O listed in Table 1. The Hg–O bond length range is constrained directly from the EXAFS results of this study, while the distance ranges of Fe–O and Al–O bonds were determined from surveys of well-characterized low-temperature and low-pressure mineral structures (see Table 1 for references). Brown and Altermatt [43] define bond valence as

$$s_{M-O} = \exp\big[(r_0 - r_{M-O})/0.37\big] \text{ valence units (vu)},$$

where s_{M-O} is the bond valence contribution in valence units (vu), r_{M-O} is the length of the metal–oxygen bond in Å, and

Table 1
Bond valence contributions for selected bonds

Bond	r_{M-O} (Å)	r_0 (Å)[a]	s_{M-O} (vu)
Fe–O	1.95–2.09[b]	1.759	0.60–0.41
	(2.02)		(0.50)
Al–O	1.86–1.94[c]	1.651	0.57–0.46
	(1.91)		(0.50)
Hg–O	2.02–2.08[d]	1.972	0.88–0.75
O–H	0.95–1.03[e]	–	0.88–0.68
O≡H	1.65–2.50[e]	–	0.13–0.25

[a] All r_0 values taken from Brown and Altermatt [43].
[b] Fe–O bond lengths as reported for goethite [64], with average value in parentheses.
[c] Al–O bond lengths as reported for bayerite [66], with average value in parentheses.
[d] Hg–O bond length range for first-neighbor O atoms as observed in this study by EXAFS spectroscopy (Tables 2–4).
[e] Bond lengths for hydroxyl (O–H) and hydrogen (O≡H) bonds as reviewed by Bargar et al. [49].

r_0 is an effective univalent bond length in Å as determined empirically from known metal oxide structures. Bond valence contributions from hydroxyl and hydrogen bonds were calculated using the following relationship derived by Bargar et al. [49]:

$$s_{OH} = 0.241/(r_{OH} - 0.677) \text{ valence units (vu)}.$$

These two equations were used to determine the bond valence saturation states of the terminal oxygen atoms at the surfaces of Fe- and Al-(hydr)oxides that serve as sites for Hg(II) sorption. By relying on the requirement that $\sum s_{M-O} = |-2.0| \pm 0.05$ vu, each Hg(II) sorption complex was assigned a relative stability level based on its deviation from this coordinatively saturated state. The results of the bond valence analyses were then compared with the Hg(II) sorption complex configurations predicted from EXAFS fitting.

In addition to this analysis, the range of Fe–O and Al–O bond lengths required to accommodate a given Hg(II) sorption complex structure and mode of surface attachment (i.e., to achieve $1.95 \leqslant \sum s_{M-O} \leqslant 2.05$ vu) was calculated for each surface complex considered. This method was utilized by Ostergren et al. [52] because it takes into account the possibility of surface relaxation and provides insight into important energetic distinctions between sites (i.e., the changes in bond length required to accommodate a given bonding arrangement).

Rearrangement of Brown and Altermatt's bond valence equation allows plausible Fe–O and Al–O bond length ranges to be calculated as

$$r_{Fe/Al-O} = r_{0,Fe/Al} - 0.37^* \ln(s_{Fe/Al-O}/n_{Fe/Al}),$$

where $s_{Fe/Al-O} = 2.0 \pm 0.05 - (\sum s_{Hg-O} + \sum s_{O-H})$ and $n_{Fe/Al}$ = the number of Fe or Al atoms bonded to the surface oxygen site. The bond length ranges determined in this manner can then be compared with the typical ranges found in well-characterized Fe- and Al-(hydr)oxide structures (1.95–2.09 Å for ^{VI}Fe(III)–O [64], 1.86–1.94 Å for

^{VI}Al(III)–O [65,66]) to identify the types of Hg(II) sorption complexes that are bonded to surface oxygens in a manner consistent with Fe–O or Al–O distances within the same ranges.

3. Results and discussion

3.1. Hg(II) sorption onto goethite

Macroscopic uptake results for Hg(II) sorbed to goethite (as well as γ-alumina and bayerite) are shown in Fig. 1. When normalized for surface area, Hg(II) uptake onto goethite results in surface coverages of $\Gamma = 0.39$–0.42 μmol/m^2 over the experimental pH range of 4.3–7.4. There is a slight decline in Hg(II) uptake with increasing pH, an effect that has been observed with other substrates [15,20–22,25,67] and that is thought to be due to the pH dependence of Hg(II) speciation. Specifically, Hg(II) uptake increases with increasing pH and reaches a maximum around pH 3 ± 1, coincident with the formation of the $Hg(OH)_2$ aqueous species as the dominant Hg phase in solution [20,24,25,68]. The pH range of the experiments conducted in the present study is above the pH of maximum sorption on goethite, so the adsorption edge typical of pH-dependent cation uptake is not observed. The slight decline in total Hg(II) uptake with increasing pH above this maximum level has been attributed to the increasing concentration of OH^- ligands with pH, which may result in the formation of less strongly sorbing aqueous complexes such as $Hg(OH)_3^-$ (Fig. 2).

Fits of the EXAFS spectra and Fourier transforms of the Hg(II)-goethite samples are shown in Fig. 3, with quantitative fitting results listed in Table 2. Both the EXAFS spectra

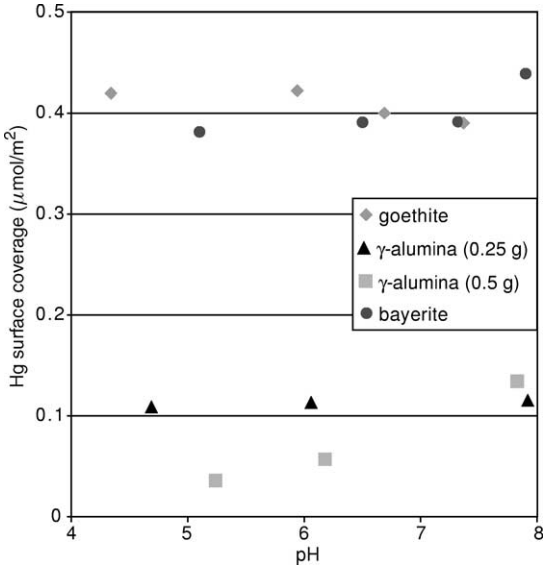

Fig. 2. Macroscopic sorption data from batch uptake of Hg(II) onto goethite, γ-alumina (using 0.5 g and 0.25 g initial solid), and bayerite. Uptake has been normalized for surface area and is expressed in μmol/m^2.

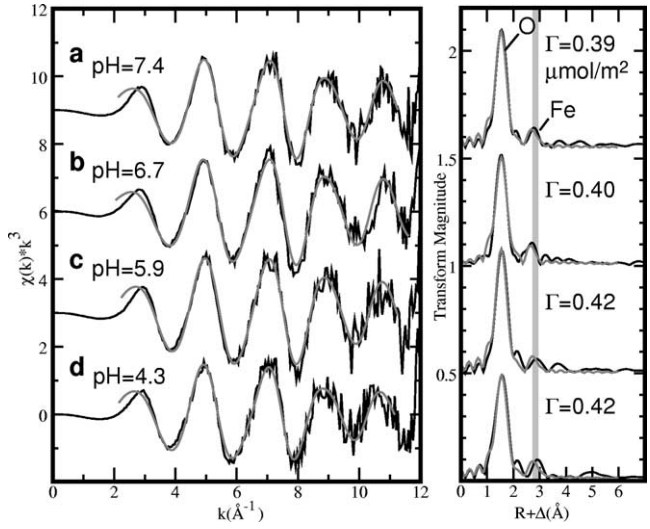

Fig. 3. Fits of the k^3-weighted EXAFS data and corresponding Fourier transforms (black = raw data, gray = fit) for Hg(II) sorbed on goethite over the pH range 4.3 to 7.4 (a–d). Uptake values (Γ in μmol/m^2) are indicated to the right of the Fourier transforms. A vertical guideline shows the Fourier transform feature consistent with second neighbor Fe atoms.

Table 2
Hg L_{III}-EXAFS fitting results for Hg(II)–goethite sorption samples (see Fig. 3 for EXAFS spectra and Fourier transforms), including coordination numbers (CN), interatomic distances (R), and Debye–Waller factors (σ^2)

Figure	pH	Hg–O			Hg–Fe		
		CN	R (Å)	σ^2 (Å^2)	CN	R (Å)	σ^2 (Å^2)
3a	7.4	2.3(1)	2.03(1)	0.005	0.5(1)	3.21(1)	0.01[a]
3b	6.7	2.4(1)	2.02(1)	0.005	0.6(1)	3.19(1)	0.01[a]
3c	5.9	2.5(1)	2.04(1)	0.006	0.4(1)	3.23(2)	0.01[a]
3d	4.3	2.4(1)	2.05(1)	0.007	0.5(1)	3.28(1)	0.01[a]

Note. Standard deviations at a 95% confidence level ($\pm 2\sigma$) are listed in parentheses.
[a] Value fixed in least-squares refinement.

and Fourier transforms of all samples studied are similar over the full pH range examined, indicating that the geometry of Hg(II) complexes and their mode of sorption onto goethite are similar for these samples. Quantitative fitting results confirm this, with all samples featuring first-shell oxygen and second-shell Fe neighbors at distances of 2.02–2.05 (± 0.01) Å and 3.19–3.28 (± 0.02) Å, respectively. The coordination numbers of the neighboring atoms are also relatively similar over this pH range (2.3–2.5 (± 0.1) for oxygen and 0.4–0.6 (± 0.2) for Fe). The Hg–O structural information for the Hg(II)–goethite samples is consistent with the coordination of Hg both in aqueous solution and in crystalline solids (e.g., HgO), as described earlier, and therefore cannot be used to distinguish between Hg(II) in the aqueous, sorbed, and solid phases. However, the Hg–Fe distance determined from EXAFS fitting supports the formation of predominantly inner-sphere sorption complexes on the goethite surface (i.e., formation of a direct chemical bond between Hg(II) and the substrate surface). By comparison, outer-sphere complexation of Hg(II) (in which Hg(II) is sur-

rounded by a solvation shell of water molecules and sorbs in a specific or nonspecific electrostatic or hydrogen-bonded manner) would yield an average Hg–Fe distance of 6.09 Å according to modeling of such a complex using the computer code Spartan Pro. The evidence from EXAFS analysis that Hg(II) sorbs in an inner-sphere mode is consistent with earlier macroscopic studies which observed little change in the pH-dependent adsorption of Hg(II) as a function of ionic strength [20,25], suggestive of inner-sphere adsorption of Hg(II) to surface functional groups on the goethite surface rather than outer-sphere sorption.

The crystal structure of goethite consists of Fe(III) ions coordinated by six O(H) ligands to form a network of edge-shared $Fe(O,OH)_6$ octahedra. The dominant crystal faces of both natural and synthetic goethite are the (110) and (021) faces [69,70]. Due to the elongation of goethite crystal growth along the *c*-axis, the (110) face of goethite accounts for approximately nine times the surface area of the (021) face [52], suggesting that the majority of Hg(II) sorption takes place at the (110) face. Assuming a simple termination of the bulk structure, the (110) face contains oxygens coordinated to one, two, or three Fe(III) ions [50]; Sposito characterizes these functional groups as A-type, C-type, and B-type, respectively [71]. The (110) face of goethite therefore presents multiple sites for Hg(II) inner-sphere sorption at the surface, including monodentate sorption to the singly, doubly, or triply coordinated oxygens and bidentate sorption to any combination of the three different types of oxygen at the surface.

All possible Hg(II) adsorption geometries on the goethite surface were modeled using Spartan Pro, with the relevant interatomic distances from the models compared to those derived from EXAFS measurements. Among the possible configurations, Hg(II) sorbed in a bidentate corner-sharing (binuclear) arrangement to A-type oxygens of two surface $Fe(O,OH)_6$ octahedra results in Hg–O and Hg–Fe interatomic distances most consistent with those determined from EXAFS fitting. Construction of a molecular model of this surface complex using Cerius[2] with an average Hg(II)–O distance of 2.04 Å and an average Fe(III)–O distance of 2.03 Å resulted in an average Hg–Fe distance of 3.28 Å (Fig. 4), which matches the EXAFS fitting analysis well. Such a configuration has two nearest neighbor oxygen atoms and two second neighbor Fe atoms. Although the predicted coordination number of oxygen based on the proposed sorption complex is consistent with the EXAFS fitting results, the predicted coordination number of iron is higher than the EXAFS-derived value. This difference was also observed by Collins et al. [39] and was interpreted as the result of some degree of Hg(II) outer-sphere sorption, therefore reducing the average number of neighboring Fe atoms at the close distance of 3.25 Å. The discrepancy may also be a function of the fixed Debye–Waller value for this atomic shell, which is strongly correlated with coordination number.

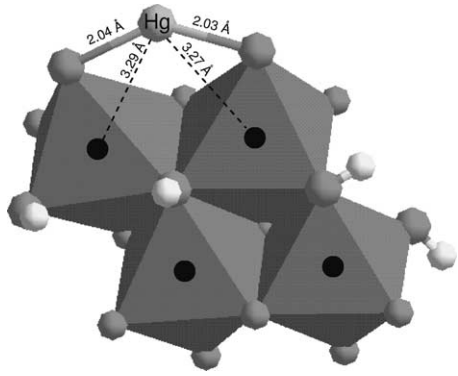

Fig. 4. Proposed Hg(II) bonding configuration on goethite, with Hg(II) sorbing as a bidentate inner-sphere complex linked in a corner-sharing (binuclear) arrangement to two A-type (i.e., singly coordinated) oxygens of adjacent $Fe(O,OH)_6$ octahedra.

Our finding that Hg(II) adsorbs dominantly as a bidentate corner-sharing complex to two surface $Fe(O,OH)_6$ octahedra on the (110) face of goethite is in agreement with Collins et al. [39], who determined the same sorption mode for Hg(II) sorbed to goethite at pH 4.6 based on EXAFS analysis and density functional calculations. The experimental results of the present study extend this proposed mode of Hg(II) sorption to the pH range 4.3–7.4, which applies more broadly to natural aquatic systems such as streams, rivers, and lakes where Hg(II) contamination may be present.

3.2. Hg(II) sorption onto γ-alumina

Figure 2 shows macroscopic uptake results for Hg(II) sorbed to γ-alumina using two different initial amounts of substrate (0.25 and 0.5 g). When 0.25 g of γ-alumina is used, uptake is essentially uniform at $\Gamma = 0.11$–0.12 μmol/m^2 over the pH range 4.7 to 7.9. This result follows the standard trend of relatively constant uptake with increasing pH above the initial Hg(II) macroscopic adsorption maximum. In contrast, when 0.5 g of γ-alumina is used, uptake increases from 0.04 to 0.13 μmol/m^2 over the pH range 5.2 to 7.8. Such a result is inconsistent with normal cation adsorption and indicates that a secondary process may be impacting Hg(II) uptake with increasing pH. In both cases, the normalized surface coverage values are considerably lower than are those of goethite and bayerite.

Figure 5 shows fits to the k^3-weighted EXAFS spectra and corresponding Fourier transforms for the sorption samples generated using 0.5 g γ-alumina (Figs. 5b–5d) and the sample containing a secondary Al precipitate (Fig. 5a). Comparison of the latter spectrum (Fig. 5a) with the sorption sample at pH 7.8 (Fig. 5b) shows clear differences, particularly in the position and shape of the third EXAFS oscillation. The equivalent oscillations in the sorption samples at pH 5.2 and 6.2 (Figs. 5c and 5d) contain contributions from both of these features. This observation suggests that the secondary Al phase that formed in the γ-alumina-free experiment also forms in the γ-alumina-bearing experiments, resulting in sorption onto two different Al phases and the additional complexity in the EXAFS spectra of the pH 5.2 and

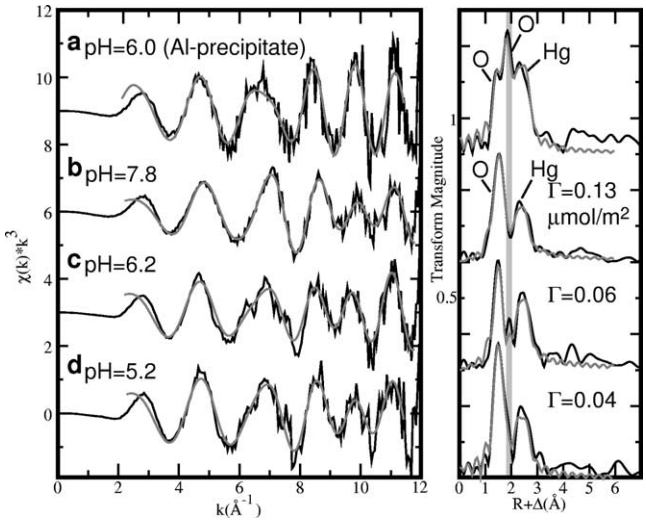

Fig. 5. Fits of the k^3-weighted EXAFS data and corresponding Fourier transforms (black = raw data, gray = fit) for Hg(II) sorbed on γ-alumina over the pH range 5.2 to 7.8 (b–d) and on a secondary Al-precipitate at pH 6.0 (a). Uptake values (Γ in μmol/m^2) are indicated to the right of the Fourier transforms. A vertical guideline shows the feature in the Fourier transforms consistent with Hg(II) sorption to a secondary Al-phase.

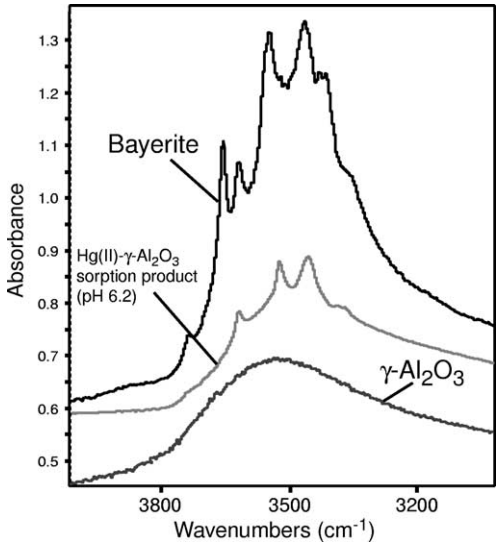

Fig. 6. Diffuse reflectance infrared Fourier transform (DRIFT) spectra of γ-alumina, bayerite, and one of the Hg(II)–alumina sorption samples generated at pH 6.2 (cf. Fig. 5c). Comparison of the spectra indicates that the alumina used in the sorption experiment has begun to transform to bayerite, a process that has been previously documented by Dyer et al. [72] and Laiti et al. [73].

6.2 sorption samples. These differences are also observed in the Fourier transforms as a distinct feature at 1.85 Å (uncorrected for phase shift) (Figs. 5a, 5c) or a slight shoulder at this distance barely visible on the high-R side of the first FT peak (Fig. 5d). The pH 7.8 sample, in comparison, lacks this additional frequency in the EXAFS and the corresponding feature in the Fourier transform.

To confirm the formation and identify of the secondary Al-containing phase during the Hg(II)–γ-alumina sorption

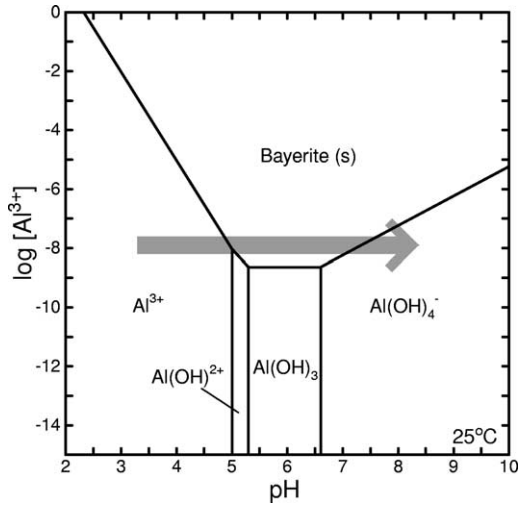

Fig. 7. Solubility diagram for bayerite generated at 25 °C and 1 atmosphere pressure using stability constants from Baes and Mesmer [9]. A pathway of increasing pH is shown (gray arrow) that would result in the formation of bayerite at pH 5.2 and 6.2 and the dissolution of bayerite by pH 7.8, as suggested by EXAFS and DRIFT data.

experiments, the DRIFT spectra of unreacted γ-alumina, unreacted bayerite, and the air-dried Hg(II)–γ-alumina sorption sample generated at pH 6.2 were compared (Fig. 6). The spectrum of the sorption sample differs from that of the pure γ-alumina and appears to be intermediate between the two end-member phases, indicating partial conversion to bayerite. This observation supports other studies of the surface hydration of γ-alumina in aqueous suspensions [72–74], which suggest that γ-alumina undergoes a surface conversion to bayerite, β-Al(OH)$_3$, over time. Specifically, these studies found that after aging γ-alumina in water for periods of 1 to 4 months, the resulting Fourier transform infrared (FTIR) spectrum shows features indicative of both γ-alumina and bayerite. Dyer et al. [72] also used X-ray diffraction (XRD) to identify both γ-alumina and bayerite in aged γ-alumina samples. These results indicate that the hydration of γ-alumina induces the formation of a bayerite layer on the surfaces of γ-alumina particles. The incomplete surface conversion of γ-alumina to bayerite in the current study indicated by the DRIFT spectra is probably a result of the short reaction time in the sorption experiments (24 h) compared to the longer aging periods of the previous FTIR studies.

The formation of a bayerite-like surface phase during the course of the sorption experiments is further supported by the solubility data for bayerite. As mentioned earlier, features in the EXAFS spectra and Fourier transforms associated with the secondary bayerite-like phase are present in the sorption samples generated at pH 5.2 (Fig. 5d) and 6.2 (Fig. 5c) yet are absent in the sorption sample generated at pH 7.8 (Fig. 5b). These results are consistent with the solubility minimum of bayerite, which occurs between pH 5.3–6.6 as seen in Fig. 7. Assuming that Al^{3+} is released to solution due to the dissolution of γ-alumina upon hydration

Table 3
Hg L_{III}-EXAFS fitting results for Hg(II)–γ-alumina sorption samples (see Fig. 5 for EXAFS spectra and Fourier transforms), including coordination numbers (CN), interatomic distances (R), and Debye–Waller factors (σ^2)

Figure	pH	Hg–O			Hg–O			Hg–Hg		
		CN	R (Å)	σ^2 (Å^2)	CN	R (Å)	σ^2 (Å^2)	CN	R (Å)	σ^2 (Å^2)
5a	6.0	0.7(1)	2.03(2)	0.005[a]	2.0(1)	2.20(1)	0.005[a]	1.1(1)	2.57(1)	0.005[a]
5b	7.8	1.3(1)	2.04(1)	0.005[a]	–	–	–	0.7(1)	2.52(1)	0.005[a]
5c	6.2	1.4(1)	2.04(1)	0.005[a]	1.3(1)	2.22(1)	0.005[a]	0.8(1)	2.56(1)	0.005[a]
5d	5.2	1.6(1)	2.05(1)	0.005[a]	1.2(1)	2.21(1)	0.005[a]	0.8(1)	2.55(1)	0.005[a]

Note. Standard deviations at a 95% confidence level ($\pm 2\sigma$) are listed in parentheses.
[a] Value fixed in least-squares refinement.

and titration to pH 3.2, increasing the pH could result in the formation of bayerite at pH 5.2 and 6.2 and the dissolution of bayerite by pH 7.8 as shown in Fig. 7. In contrast, the sorption samples generated using 0.25 g initial substrate feature constant Hg(II) uptake as a function of pH (Fig. 2), indicating that bayerite formation and its effect on Hg sorption are not as significant at this reduced solids concentration. The use of less initial substrate may have resulted in a lower degree of dissolution and release of Al^{3+} to solution, driving the reaction pathway in Fig. 7 below the solubility limit of bayerite and inhibiting precipitation of a secondary phase during the time period of the experiments.

Given that both γ-alumina and a secondary bayerite-like phase are present in this sorption system, sorption to both substrates was considered in the analysis of the Hg–γ-alumina EXAFS data. Fitting the EXAFS spectra of all samples (Table 3) yields Hg–O and Hg–Hg neighbors at distances of 2.03–2.05 ($\pm$0.02) Å and 2.52–2.57 ($\pm$0.01) Å, respectively. The samples containing EXAFS features that correlate with the presence of the bayerite-like phase (Figs. 5a, 5c, and 5d) indicate an additional O neighbor at a distance of 2.20–2.22 ($\pm$0.01) Å, while the pH 7.8 sample (Fig. 5b) lacks this Hg–O pair correlation. The average Hg–O distance of 2.21 ($\pm$0.01) Å does not correspond to any of the Hg(II) hydrolysis products described earlier or the Hg–O distances in solids such as montroydite (HgO, which features Hg–O distances of 2.03 and 2.82 Å) [75] and is suggestive of direct inner-sphere sorption on the bayerite-like phase. However, proof of this mode of sorption would require observation of second neighbor Al atoms at a distance corresponding to a reasonable surface bonding geometry. Such second neighbors were not observed in this study, possibly due to interference from the Hg–Hg pair correlation as described later in this section.

The presence of binuclear Hg complexes, with an average Hg–Hg distance of 2.54 ($\pm$0.01) Å determined from EXAFS fitting, is unexpected at such low Hg surface coverages and does not correlate with typical Hg–Hg interatomic distances in Hg(II) solids (e.g., 3.30 and 3.59 Å in montroydite [75]) or polynuclear aqueous Hg(II) species such as Hg_2OH^{3+} and $Hg_2(OH)_2^{2+}$, (average Hg–Hg distances of 3.64 Å) [12,13]. In these cases, a bridging oxygen atom is located between the proximate Hg atoms, resulting in the larger Hg–Hg distance observed in Hg(II)-containing phases. For similar reasons, the formation of a mixed-metal hydrotalcite phase, as found in EXAFS studies of Co(II), Ni(II), and Zn(II) sorption on Al (hydr)oxides and clays [76–79], or of multinuclear sorption complexes, as observed in EXAFS studies of Pb(II) and Cr(III) sorption on γ-alumina [80,81], would also produce Hg–Hg distances longer than those derived from EXAFS fitting. Additionally, the large ionic radius and coordination chemistry of Hg(II), with its tendency to be two-coordinated, would likely preclude incorporation of Hg(II) into an ordered hydrotalcite-like phase containing both Al and Hg. A review of the literature did not identify any Hg(II) aqueous species or compounds with Hg–Hg distances at 2.54 Å, as determined from EXAFS fitting of the spectra; such a short interatomic distance could only result from direct Hg(II)–Hg(II) bonding, which has not been observed in any known system.

Hg–Hg distances consistent with those derived from the EXAFS fits in this study are common, however, in species containing the mercurous Hg(I) ion, which forms binuclear complexes featuring a direct Hg–Hg bond with distances ranging from 2.43 to 2.69 Å [82,83] and averaging 2.50 Å [9,10]. The initial Hg added to the sorption experiments was in the 2+ oxidation state, though, as confirmed by Raman microscopy (see Section 2). Assuming that the EXAFS-derived Hg–Hg distance of 2.54 Å represents a Hg(I) species and not some unknown Hg(II) species, reduction of Hg(II) to Hg(I) must have occurred either during the course of the uptake experiment or during EXAFS data collection. Possible causes for Hg(II) reduction include the bubbling of N_2 through the experimental system, driving the dissolved O_2 concentration down and generating a sufficiently anoxic environment to reduce Hg(II) to Hg(I) when introduced to the system at $\sim$pH 3.2 (Fig. 8). However, Hg(I) as Hg_2^{2+} is not dominant above pH 4 (although thermodynamic data are not available for the $Hg_2(OH)_2$ hydrolysis product which was observed at higher pH levels [84,85]), indicating that the reducing environment is not the sole explanation for the apparent presence of Hg(I) species in the sorption samples generated. X-ray-induced photoreduction during EXAFS collection, which has been observed in XPS and XAS experiments in other systems containing chromium, cobalt, copper, and iron [86–89], may play a more significant role in the reduction of Hg(II) to Hg(I) over the pH range 5.2 to 7.8. Additionally, the evidence for Hg(I) species is unique

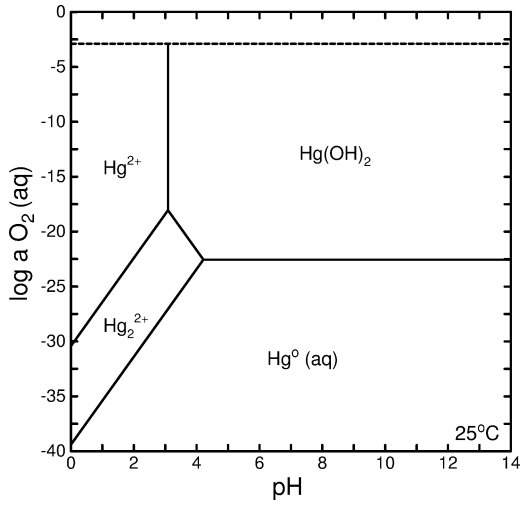

Fig. 8. Fields of stability for aqueous Hg species at 25 °C and 1 atmosphere pressure, plotting dissolved oxygen versus pH and using stability constants from Baes and Mesmer [9]. In the N_2 environment of the sorption experiments, dissolved oxygen concentrations may decrease to the point where the reduced Hg(I) mercurous ion, as Hg_2^{2+}, is stable when Hg is introduced into the system at ∼pH 3.2.

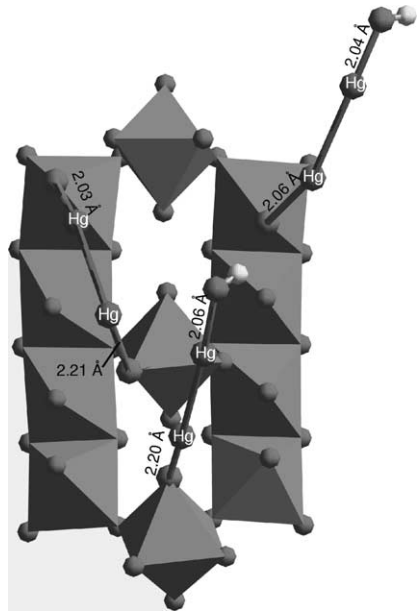

Fig. 9. Proposed bonding configurations of Hg(II) to the hydrated γ-alumina surface, with reduced Hg(I)–Hg(I) binuclear species sorbing as (1) a monodentate (mononuclear) complex on a singly coordinated oxygen (upper right); (2) a bidentate corner-sharing (binuclear) complex on two singly coordinated oxygens (upper left); and (3) a monodentate (mononuclear) complex on a singly coordinated oxygen site of a bridging hydrated Al octahedron (bottom center). Not shown is outer-sphere sorption of the $Hg_2(OH)_2$ aqueous species. The Hg(I)–Hg(I) distance is 2.54 Å in all cases.

to Hg(II) sorption on γ-alumina (and not to Hg(II) sorption on goethite or bayerite), suggesting that some property of the γ-alumina substrate (e.g., its surface conversion to bayerite or the low total uptake onto the substrate, resulting in a higher proportion of free Hg(II) in solution) may facilitate this process. However, no clear explanation for such a mechanism is apparent.

Modeling of the EXAFS spectra of Hg on the hydrated γ-alumina surface is complicated by several factors, including (1) conversion of the γ-alumina surface to bayerite or a bayerite-like phase; (2) the incomplete nature of this conversion in the sorption experiments due to the short reaction times, resulting in both bayerite and γ-alumina at the surface; and (3) lack of a definitive structural model for the hydrated γ-alumina surface and the mechanism of transformation to bayerite. Several studies have found that once exposed to water, the $Al(O,OH)_4$ tetrahedra at the γ-alumina surface undergo rapid hydroxylation, resulting in only surface $Al(O,OH)_6$ octahedra [47,80,90]. The presence of Al octahedra at the surfaces of both bayerite and γ-alumina in contact with water was assumed in modeling Hg surface complexes in the Hg–γ-alumina sorption experiments.

A model of the assumed structure of the hydrated γ-alumina surface was constructed by converting the bridging Al tetrahedra to Al octahedra at the (001) face of γ-alumina (which is identical to the (100) and (010) faces). This face contains singly, doubly, and triply coordinated oxygen sites to which Hg(I), present as the $Hg_2(OH)_2$ aqueous species, may sorb. All potential inner-sphere adsorption geometries of $Hg_2(OH)_2$ on the modified γ-alumina (001) surface were modeled using Spartan Pro, with the relevant interatomic distances from the models compared to those derived from EXAFS measurements. The average first neighbor Hg–O distance of 2.04 (±0.02) Å and the average Hg–Hg distance of 2.54 (±0.01) Å are consistent with sorption of Hg in several modes to several types of surface sites, including monodentate mononuclear sorption to both singly and doubly coordinated oxygen sites, bidentate sorption in both corner-sharing (binuclear) and edge-sharing (mononuclear) arrangements, and nonspecific sorption as outer-sphere complexes. However, the majority of bidentate sorption complexes require an unreasonable distortion of the linear binuclear $Hg_2(OH)_2$ species (i.e., edge-sharing bidentate complexes require the Hg–Hg–O angle to be altered from 180° to 95°–100°) and are therefore unlikely to represent dominant modes of sorption. By comparison, monodentate sorption complexes do not place such angular constraints on the sorbing Hg_2^{2+} complex and are more consistent with the distances and coordination numbers determined from EXAFS fitting. This is demonstrated by the monodentate mononuclear sorption species in Fig. 9 (top right), which features Hg–O distances of 2.04–2.06 Å and a Hg–Hg distance of 2.54 Å.

Hg–Al interactions which may distinguish inner-sphere complexes (Hg–Al distance = ∼3.0–3.5 Å) from outer-sphere complexes (Hg–Al distance >4 Å) were not detected in the EXAFS spectra or the Fourier transforms. One possible interpretation is that Hg(I) is present primarily as outer-sphere complexes, which may explain the relatively low uptake of Hg by the γ-alumina substrate compared with the degree of uptake on goethite and bayerite, in which Hg

forms primarily inner-sphere complexes. Outer-sphere sorption would also be consistent with the increasing Hg uptake observed as pH approaches the pH_{pzc} of Al oxides (≈9). Another possible interpretation is that Hg(I) sorbs in an inner-sphere fashion but the Hg–Hg pair correlation, which produces a relatively broad feature in the Fourier transforms between 2 and 3 Å (uncorrected for phase shift) and strong amplitude in the EXAFS spectra at k values greater than 7 $Å^{-1}$ (Fig. 5), results in interference with the lower amplitude EXAFS frequencies resulting from the Hg–Al pair correlations. Therefore, both outer-sphere sorption and inner-sphere monodentate surface complexation are considered as possible modes of uptake for Hg–γ-alumina sorption samples based on the EXAFS-derived first-neighbor Hg–O and Hg–Hg distances.

The features in both the EXAFS spectra and Fourier transforms corresponding to the Hg–O pair correlation with an average distance of 2.21 (±0.01) Å appear most prominently in the secondary Al-precipitate and are also visible in the two sorption samples generated at pH levels around the solubility minimum of bayerite. As discussed above, a hydrated γ-alumina structural model was used to help constrain the mode(s) of attachment of Hg(I) binuclear sorption complexes. Among the sorption modes tested, one bidentate corner-sharing and one monodentate sorption complex yield Hg–O distances of 2.21 and 2.20 Å, respectively; additionally, both complexes involve sorption to the bridging Al octahedra of the hydrated γ-alumina surface (Fig. 9).

3.3. Hg(II) sorption onto bayerite

Macroscopic uptake of Hg(II) onto bayerite (Fig. 2) is relatively constant over the pH range 5.1–7.9, with surface coverages ranging from 0.39 to 0.44 μmol/m^2. When normalized for surface area, Hg(II) uptake onto bayerite is comparable to Hg(II) uptake on goethite (0.39–0.42 μmol/m^2). The relatively low surface area of the bayerite compared with those of goethite and γ-alumina resulted in reduced total Hg(II) uptake and poorer quality EXAFS spectra for the Hg(II)–bayerite samples (Fig. 10). However, the Fourier transforms are similar enough to imply that the mode(s) of sorption are similar over the pH range examined.

The EXAFS fitting results listed in Table 4 reflect this interpretation, yielding consistent first-neighbor oxygen distances of 2.02–2.07 (±0.01) Å and Al neighbors at distances of 3.06–3.09 (±0.02) and 3.35–3.40 (±0.03) Å for all samples. As with Hg L_{III}-EXAFS data from the Hg sorption samples involving the other substrates, the first-neighbor oxygen distance and coordination number determined from EXAFS fitting are not unique enough to distinguish between aqueous, sorbed, or precipitated Hg(II). However, the average Hg–Al distances (3.07 and 3.39 Å) do indicate inner-sphere Hg(II) sorption on bayerite (outer-sphere Hg(II) sorption would result in an average Hg–Al distance of 6.52 Å based on Spartan Pro modeling). The bayerite crystal structure consists of Al(III) ions coordinated by six O(H) ligands to form sheets of edge-sharing $Al(O,OH)_6$ octahedra arranged in interlinking six-membered rings oriented parallel to the (001) face [66]. Assuming that the (001) surface is a simple termination of the bulk structure, this arrangement provides surface oxygen sites that are coordinated to either one or two Al(III) ions. Based on such a model, there are many potential inner-sphere sorption geometries for Hg(II) on the bayerite surface, including monodentate sorption to either the singly or doubly coordinated oxygens and biden-

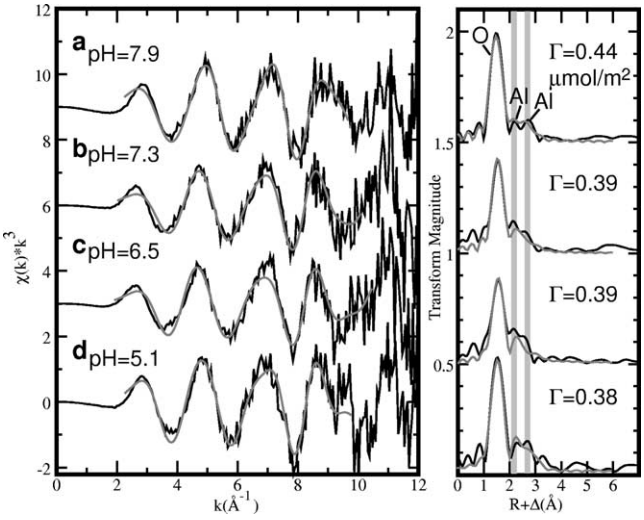

Fig. 10. Fits of the k^3-weighted EXAFS data and corresponding Fourier transforms (black = raw data, gray = fit) for Hg(II) sorbed on bayerite over the pH range 5.1 to 7.9 (a–d). Uptake values (Γ in μmol/m^2) are indicated to the right of the Fourier transforms. Vertical guidelines show Fourier transform features corresponding to the second-neighbor Al atoms.

Table 4
Hg L_{III}-EXAFS fitting results for Hg(II)–bayerite sorption samples (see Fig. 10 for EXAFS spectra and Fourier transforms), including coordination numbers (CN), interatomic distances (R), and Debye–Waller factors (σ^2)

Figure	pH	Hg–O			Hg–Al			Hg–Al		
		CN	R (Å)	σ^2 (Å^2)	CN	R (Å)	σ^2 (Å^2)	CN	R (Å)	σ^2 (Å^2)
10a	7.9	1.9(1)	2.02(1)	0.005	0.8(2)	3.06(2)	0.01[a]	1.1(2)	3.40(2)	0.01[a]
10b	7.3	1.7(2)	2.06(1)	0.004	1.1(2)	3.07(2)	0.01[a]	0.8(3)	3.39(3)	0.01[a]
10c	6.5	1.9(2)	2.07(1)	0.006	1.6(3)	3.07(1)	0.01[a]	1.1(4)	3.35(2)	0.01[a]
10d	5.1	2.2(2)	2.07(1)	0.007	1.6(3)	3.09(1)	0.01[a]	1.7(4)	3.39(2)	0.01[a]

Note. Standard deviations at a 95% confidence level (±2σ) are listed in parentheses.
[a] Value fixed in least-squares refinement.

tate sorption to various combinations of the two types of oxygens.

All Hg(II) inner-sphere adsorption geometries on the bayerite (001) surface were modeled using Spartan Pro, with the relevant interatomic distances from the models compared with those derived from EXAFS measurements. Among possible sorption complexes, three particular Hg(II) configurations, two bidentate and one monodentate, result in Hg–Al distances that are consistent with the values determined from EXAFS fitting (Fig. 11). One possible complex has Hg(II) sorbed as a bidentate edge-sharing (mononuclear) complex to two singly coordinated oxygens. A second possible complex has Hg(II) sorbed as a bidentate corner-sharing (binuclear) complex to two singly coordinated oxygens. A third possible complex has Hg(II) sorbed as a monodentate (mononuclear) complex to a singly coordinated (i.e., terminal or nonbridging) oxygen site. All three complexes have Hg–O distances between 2.03 and 2.08 Å, which are consistent with EXAFS fitting results. The Hg–Al distance of the bidentate edge-sharing complex (3.01 Å) is close to that determined from EXAFS fitting (3.06–3.09 (±0.02) Å), while the Hg–Al distances of the bidentate corner-sharing (3.35 Å) and monodentate (3.42 Å) complexes are consistent with the EXAFS-determined Hg–Al distance of 3.35–3.40 (±0.03) Å. We therefore conclude that the three proposed complexes are all possible modes of Hg(II) inner-sphere sorption to bayerite. Finally, the EXAFS data and fitting results of the Hg(II)–bayerite system are significantly different from those of the Hg(II) sorption samples generated with γ-alumina, supporting the assumption that the surface conversion to bayerite in the latter system is incomplete and that sorption under those conditions is best modeled using the hydrated γ-alumina surface.

3.4. Bond valence calculations

Results from bond valence analyses of various Hg sorption complex geometries on the surfaces of Fe and Al (hydr)oxides are presented in Table 5. A number of possible Hg sorption complexes on Fe- and Al-(hydr)oxides are considered and listed in the first column of Table 5. These complexes represent the range of potential Hg configurations on goethite, γ-alumina, and bayerite based on the possible surface oxygen sites of the three substrates as described in earlier sections. To summarize, the goethite (110) face contains oxygens that are singly coordinated (A-type, represented in Table 5 as species beginning with "Fe–O…"), doubly coordinated (C-type, represented as "Fe_2–O…"), and triply coordinated (B-type, represented as "Fe_3–O…"). Similarly, γ-alumina contains oxygens with the same range of coordinations to Al(III) ions (represented as "Al–O…," "Al_2–O…," and "Al_3–O…"). Bayerite contains only singly and doubly coordinated oxygen sites.

Listed in the second and third columns are the bond valence sums of the oxygens both with and without bond valence contributions of hydrogen bonds. In order to determine

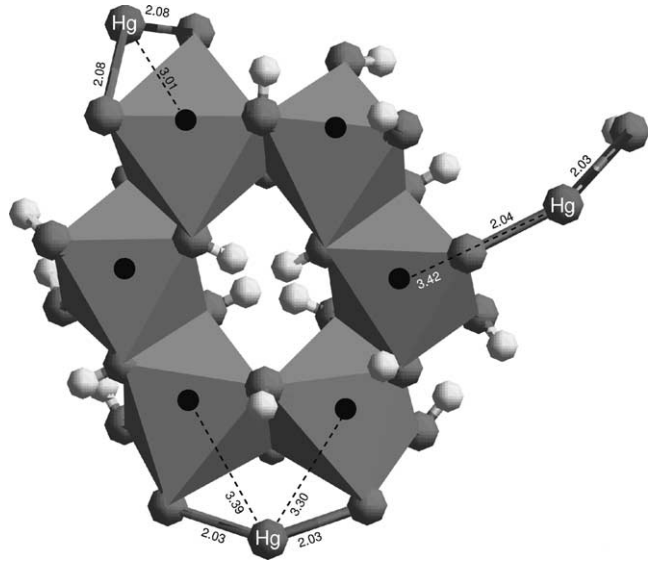

Fig. 11. Proposed bonding configurations of Hg(II) to bayerite, with Hg(II) sorbing as (1) a bidentate edge-sharing (mononuclear) complex on two singly coordinated oxygens (upper left); (2) a bidentate corner-sharing (binuclear) complex on two singly coordinated oxygens (bottom center); and (3) a monodentate (mononuclear) complex on a singly coordinated oxygen site (upper right).

the number of hydrogen bonds that may exist for any given surface oxygen, it is assumed that the maximum coordination number for oxygen is 4 (including hydrogen bonds), as observed for oxygen in aqueous solution and ice [91]. Therefore, oxygen atoms that are already four-coordinated (e.g., Fe_2–OH–Hg, Al_3–O–Hg) require no additional hydrogens and, therefore, have the same bond valence sums in the two columns. The oxygen coordinative state, listed in the fourth column, is classified as saturated if $1.95 \leqslant \sum s_{\mathrm{M-O}} \leqslant 2.05$ vu, undersaturated if $\sum s_{\mathrm{M-O}} < 1.95$ vu, and oversaturated if $\sum s_{\mathrm{M-O}} > 2.05$ vu. Listed in the fifth column are the Fe–O and Al–O bond length ranges predicted using bond valence constraints imposed by the formation of each Hg(II) sorption complex. Comparison of these ranges for each Hg(II) sorption complex with the observed ranges for $Fe(O,OH)_6$ octahedra (1.95–2.09 Å) or $Al(O,OH)_6$ octahedra (1.86–1.94 Å) can then predict whether the complex is stable within the structural constraints of the Fe and Al (hydr)oxide substrates used. Consideration of both the coordinative saturation state of the surface oxygen site and the Fe–O or Al–O bond length can then be used to determine which Hg(II) sorption complexes are plausible or unlikely.

Based on this analysis, Hg(II) sorption complexes that are not likely to exist due to either the coordinative saturation levels of the surface oxygen sites or unrealistic lengthening or shortening of Fe–O or Al–O bond lengths can be readily identified. The remaining species (listed in Table 5 in bold) generally meet the requirements of coordinatively saturated surface oxygen atoms and Fe–O or Al–O bond length ranges that are compatible with those of typical Fe and Al (hydroxides). Of these species, those that correlate with the inner-sphere complexes predicted from

Table 5
Bond valence analyses for Hg(II) bonding to surface functional groups on Fe and Al (hydr)oxides[a]

Surface species/bonds	$\sum s_{M-O}$ at oxygen (vu)		Oxygen coordination state	$r_{Fe/Al-O,bv}$ (Å)	Prediction
	No H-bonds	With H-bonds			
Fe–O–Hg	**1.16–1.48**	**1.42–1.97**	**Saturated**	**1.66–1.96**[c]	**Stable**
Fe–OH–Hg	**1.84–2.36**	**1.97–2.61**	**Saturated**	**1.94–2.94**[c]	**Stable**
Fe–OH_2–Hg	2.52–3.24	2.52–3.24	Oversaturated	>2.32[b]	Doesn't occur
Fe_2–O–Hg	**1.56–2.07**	**1.70–2.32**	**Saturated**	**1.92–2.09**[c]	**Stable**
Fe_2–OH–Hg	2.25–2.95	2.25–2.95	Oversaturated	2.19–2.63	Doesn't occur
Fe_3–O–Hg	**1.97–2.67**	**1.97–2.67**	**Saturated**	**2.07–2.14**[c]	**Stable**
Al–O–Hg	**1.20–1.45**	**1.47–1.94**	**Undersaturated**	**1.66–1.96**[d]	**Plausible**
Al–OH–Hg	**1.89–2.33**	**2.02–2.58**	**Saturated**	**1.94–2.94**[d]	**Stable**
Al–OH_2–Hg	2.57–3.21	2.57–3.21	Oversaturated	>1.98[b]	Doesn't occur
Al_2–O–Hg	**1.66–2.02**	**1.79–2.26**	**Saturated**	**1.92–2.09**[d]	**Stable**
Al_2–OH–Hg	2.35–2.90	2.35–2.90	oversaturated	2.19–2.63	Doesn't Occur
Al_3–O–Hg	2.12–2.58	2.12–2.58	oversaturated	2.07–2.14	Doesn't Occur

[a] Rows in bold indicate conditions suitable for Hg(II) binding.
[b] Limit imposed by the maximum range of Fe–O or Al–O bond lengths observed in mineral structures [64,66].
[c] Distance range overlaps that of Fe (hydr)oxides (Fe–O = 1.95–2.09 Å).
[d] Distance range overlaps that of Al (hydr)oxides (Al–O = 1.86–1.94 Å).

EXAFS fitting are classified as stable or plausible. Specifically, the bidentate corner-sharing complex proposed in the Hg(II)–goethite sorption system would require Fe–O–Hg or Fe–OH–Hg species and the additional hydrogen bonding required to achieve four-coordinated oxygen atoms as described earlier. Both of these surface species feature coordinatively saturated surface oxygen atoms according to bond valence principles. Similarly, the monodentate and bidentate corner-sharing and edge-sharing complexes proposed from fitting EXAFS results in the Hg(II)–bayerite and Hg(I)–γ-alumina sorption systems would involve Al–O–Hg, Al–OH–Hg, and Al_2–O–Hg species. Once hydrogen bonding is taken into account, these particular sorption species are also stable from a bond valence perspective, providing good agreement between the two techniques. Additional species (Fe_2–O–Hg and Fe_3–O–Hg) are also stable according to bond valence constraints, but the specific sorption arrangements (e.g., bidentate edge-sharing on goethite) are not supported by the results of EXAFS fitting. This implies that at best these configurations may exist as minor sorption species only.

3.5. Natural samples

EXAFS spectra and Fourier transforms of the sorption samples generated using natural fine-grained precipitates (Knoxville Fe-(hydr)oxide and Sulphur Bank Al/Si floc) are shown in Fig. 12. Spectral data for sorption samples of Hg(II)–goethite and Hg(II)–bayerite at similar pH values are also shown for comparison. Qualitative similarities are apparent in both the EXAFS spectra and the Fourier transforms of the Knoxville Fe-(hydr)oxide sorption sample (Fig. 12b) and the goethite sorption sample (Fig. 12a). Similarities are also observed between the EXAFS spectra and Fourier transforms of the Sulphur Bank Al/Si floc sorption sample (Fig. 12d) and the bayerite sorption sample (Fig. 12c). The

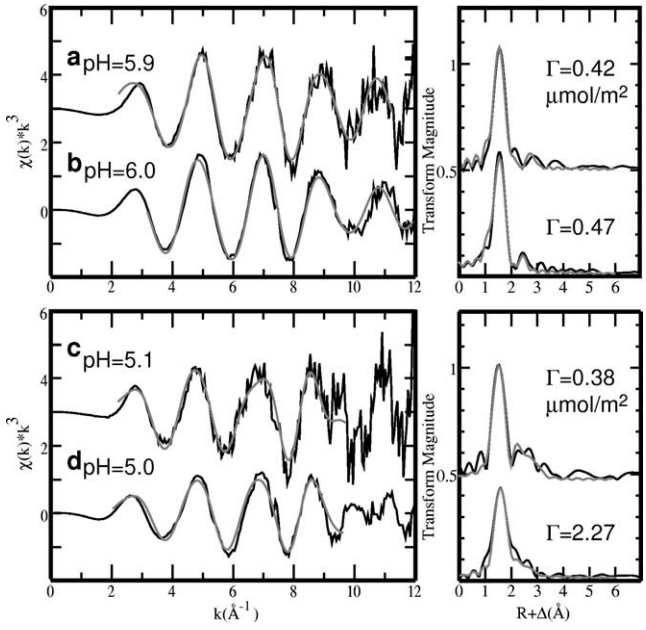

Fig. 12. Fits of the k^3-weighted EXAFS data and corresponding Fourier transforms (black = raw data, gray = fit) for Hg(II) sorbed on the following synthetic and natural substrates: (a) goethite (repeated from Fig. 2c); (b) Knoxville Fe-hydroxide precipitate; (c) bayerite (repeated from Fig. 6d); and (d) Sulphur Bank Al/Si flocculent. Uptake values (Γ in μmol/m^2) are indicated to the right of the Fourier transforms.

Hg(II) sorption densities on the Knoxville Fe-(hydr)oxide and goethite are comparable when normalized for surface area (Γ = 0.42 and 0.47 μmol/m^2, respectively). However, Hg(II) uptake is enhanced on the Al/Si floc (Γ = 2.27 μmol/m^2) relative to bayerite (Γ = 0.38 μmol/m^2). This Hg-hyperaccumulating property of the floc has been noted at the Sulphur Bank mine site, where methylmercury (MeHg) concentrations in the floc are found to be an order of magnitude higher than in surrounding sediments [92].

Table 6
Hg L_{III}-EXAFS fitting results for Hg(II)-natural substrate samples (see Fig. 12 for spectra and Fourier transforms). Fitting results of sorption samples using synthetic model substrates have been included for comparison. Results include coordination numbers (CN), interatomic distances (R), and Debye–Waller factors (σ^2)

Figure	Substrate	pH	Hg–O			Hg–Fe					
			CN	R (Å)	σ^2 (Å^2)	CN	R (Å)	σ^2 (Å^2)			
12a	Goethite	5.9	2.5(1)	2.04(0)	0.006	0.4(1)	3.23(2)	0.01[a]			
12b	Knoxville Fe-precipitate	6.0	3.0(1)	2.03(0)	0.008	0.3(1)	2.84(1)	0.01[a]			
			Hg–O			Hg–Al			Hg–Al		
12c	Bayerite	5.1	2.2(2)	2.07(1)	0.007	1.6(3)	3.09(1)	0.01[a]	1.7(4)	3.39(2)	0.01[a]
12d	Sulphur Bank Al/Si floc	5.0	1.7(1)	2.07(0)	0.005	0.5(1)	3.10(2)	0.01[a]	0.7(2)	3.41(2)	0.01[a]

Note. Standard deviations at a 95% confidence level ($\pm 2\sigma$) are listed in parentheses.
[a] Value fixed in least-squares refinement.

Table 6 shows EXAFS fitting results for Hg(II) sorbed on the natural samples and goethite and bayerite, providing quantitative confirmation of the similarities apparent in the EXAFS spectra and Fourier transforms. While the interatomic distances derived from the Hg(II)–bayerite sample and the Sulphur Bank floc are comparable, the Hg–Fe distance calculated for the Hg(II) Knoxville substrate is considerably shorter (by 0.39 Å) than that of the Hg(II)–goethite sample. The amorphous and heterogeneous nature of natural substrates may contribute to this difference, as the presence of multiple potential sorption sites would result in increasing disorder among second and more distant neighbors. Hg(II) could also sorb in a different mode to other Fe (hydr)oxide phases structurally distinct from goethite such as ferrihydrite, resulting in the shorter Hg–Fe distance observed. Despite these complicating factors, the spectral similarities between the natural and model sorbents indicate that the types of Hg(II) sorption complexes and the modes of Hg(II) sorption are similar. Thus, the synthetic goethite and bayerite appear to be useful surrogates of the more complex natural samples from the Sulphur Bank and Knoxville mines in terms of understanding Hg(II) sorption processes in environmental systems.

4. Summary

A combination of macroscopic, spectroscopic, and bond valence analyses has led to an improved molecular-scale understanding of Hg(II) sorption on Fe- and Al-(hydr)oxides. EXAFS data indicate that Hg(II) forms inner-sphere sorption complexes to goethite and bayerite over pH ranges (4–8) consistent with those of most natural aquatic systems; outer-sphere complexation may also be a significant component of Hg uptake on γ-alumina. Goethite was found to sorb Hg(II) primarily as a bidentate sorption complex in a corner-sharing arrangement to the $Fe(O,OH)_6$ octahedra of the goethite surface (likely to the (110) face, which accounts for the majority of the surface area of the goethite particles used in this study). Hg(II) sorbs dominantly in bidentate corner-sharing, bidentate edge-sharing, and monodentate modes to the $Al(O,OH)_6$ octahedra at the bayerite surface. The interpretation of Hg sorption on γ-alumina was complicated by the surface hydration/conversion to a bayerite-like phase during the course of the sorption experiments and the reduction of Hg(II) to Hg(I) dimers during EXAFS data collection. Hg–Al interactions were not directly observed in the EXAFS data for the Hg(II)–γ-alumina system, precluding conclusive identification of inner-sphere complexes in this system. However, the observed Hg–O distance at 2.20 Å is consistent with Hg(I) species bonded to the $Al(O,OH)_6$ octahedra of the hydrated γ-alumina surface as both monodentate and bidentate corner-sharing complexes. In addition, Hg(I) may form outer-sphere complexes on the γ-alumina surface. The inner-sphere sorption geometries as determined from EXAFS analysis and modeled with Cerius[2] and Spartan Pro are consistent with bond valence calculations.

Molecular-scale studies of Hg(II) uptake to mineral surfaces in controlled model systems provide an important foundation for understanding Hg(II) sorption mechanisms in contaminated natural systems. The similarities between Hg(II) sorption on synthetic, homogeneous substrates and on fine-grained Fe and Al precipitates such as those found at the Knoxville and Sulphur Bank mines support this assertion. Characterizing these processes in settings where Hg contamination is a concern provides an understanding of some of the molecular-scale processes responsible for the sequestration of Hg in sediments and the possible remobilization of sorbed Hg in aquatic systems that impact its potential bioavailability.

Acknowledgments

We thank the staff of the Stanford Synchrotron Radiation Laboratory (SSRL) particularly John Bargar and Joe Rogers, for their assistance during the EXAFS data collection. SSRL is supported by the Department of Energy (Office of Basic Energy Sciences and Office of Health and Environmental Sciences) and the National Institutes of Health. Guangchou Li (Stanford University) provided support in conducting the ICP analyses. Ben Bostick (Stanford University) is thanked

for his help with the DRIFT and Raman spectral analyses as well as for useful discussions about EXAFS interpretation. This study was supported by the U.S. Environmental Protection Agency Science to Achieve Results program (U.S. EPA-STAR Program Grant EPA-R827634-01-1) and the U.S. Geological Survey, Geologic Division.

References

[1] W.F. Fitzgerald, D.R. Engstrom, R.P. Mason, E.A. Nater, Environ. Sci. Technol. 32 (1998) 1.
[2] T.A. Jackson, Environ. Rev. 5 (1997) 99.
[3] E.B. Swain, D.R. Engstrom, M.E. Brigham, T.A. Henning, P.L. Brezonik, Science 257 (1992) 784.
[4] H. Sakamoto, T. Tomiyasu, N. Yonehara, Geochem. J. 29 (1995) 97.
[5] M.O. Barnett, L.A. Harris, R.R. Turner, T.J. Henson, R.E. Melton, R.J. Stevenson, Water Air Soil Pollut. 80 (1995) 1105.
[6] C.S. Kim, G.E. Brown Jr., J.J. Rytuba, Sci. Total Environ. 261 (2000) 157.
[7] C.S. Kim, J.J. Rytuba, G.E. Brown Jr., Appl. Geom., in press.
[8] J.D. Hem, Chemical Behavior of Mercury in Aqueous Media, U.S. Geological Survey, 1970.
[9] C.F. Baes, R.E. Mesmer, The Hydrolysis of Cations, Krieger, Malabar, FL, 1976.
[10] D.T. Richens, The Chemistry of Aqua Ions, Wiley, New York, 1997.
[11] D.W. Barnum, Inorg. Chem. 22 (1983) 2297.
[12] G. Johansson, Acta Chem. Scand. 25 (1971) 2799.
[13] G. Johansson, Acta Chem. Scand. 25 (1971) 2787.
[14] F.A. Cotton, G. Wilkinson, Advanced Inorganic Chemistry, Wiley, New York, 1988.
[15] D. Sarkar, M.E. Essington, K.C. Misra, Soil Sci. Soc. Am. J. 64 (2000) 1968.
[16] T. Viraraghavan, A. Kapoor, Appl. Clay Sci. 9 (1994) 31.
[17] J.S. Wang, P.M. Huang, U.T. Hammer, W.K. Liaw, Appl. Clay Sci. 1 (1985) 125.
[18] H. Farrah, W.F. Pickering, Water Air Soil Pollut. 9 (1978) 23.
[19] D.W. Newton, R. Ellis, G.M. Paulsen, J. Environ. Qual. 5 (1976) 251.
[20] D. Sarkar, M.E. Essington, K.C. Misra, Soil Sci. Soc. Am. J. 63 (1999) 1626.
[21] L. Gunneriusson, S. Sjoberg, J. Colloid Interface Sci. 156 (1993) 121.
[22] N.J. Barrow, V.C. Cox, J. Soil Sci. 43 (1992) 295.
[23] D.G. Kinniburgh, M.L. Jackson, Soil Sci. Soc. Am. J. 42 (1978) 45.
[24] R.A. Lockwood, K.Y. Chen, Environ. Lett. 6 (1974) 151.
[25] M.G. MacNaughton, R.O. James, J. Colloid Interface Sci. 47 (1974) 431.
[26] C. Tiffreau, J. Lutzenkirchen, P. Behra, J. Colloid Interface Sci. 172 (1995) 82.
[27] Y. Yin, H.E. Allen, C.P. Huang, Environ. Sci. Technol. 31 (1997) 496.
[28] N.J. Barrow, V.C. Cox, J. Soil Sci. 43 (1992) 305.
[29] T.D. Obukhovskaya, Sov. Soil Sci. 14 (1982) 49.
[30] R.S. Reimers, P.A. Krenkel, J. Water Pollut. Control Fed. 46 (1974) 352.
[31] E. Schuster, Water Air Soil Pollut. 45 (1991) 667.
[32] T.J. Hogg, J.W.B. Stewart, J.R. Bettany, J. Environ. Qual. 7 (1978) 440.
[33] K. Schluter, Environ. Geol. 30 (1997) 266.
[34] S. Ramamoorthy, B.R. Rust, Can. J. Earth Sci. 13 (1976) 530.
[35] F.E. Huggins, G.P. Huffman, G.E. Dunham, C.L. Senior, Energy Fuels 13 (1999) 114.
[36] J. Lakatos, S.D. Brown, C.E. Snape, Energy Fuels 13 (1999) 1046.
[37] W. Stumm, J.J. Morgan, Aquatic Chemistry: An Introduction Emphasizing Chemical Equilibria in Natural Waters, Wiley, New York, 1996.
[38] J.R. Bargar, P. Persson, G.E. Brown, J. Phys. IV Colloque C 2 (1997) 825.
[39] C.R. Collins, D.M. Sherman, K.V. Ragnarsdottir, J. Colloid Interface Sci. 219 (1999) 345, doi:10.1006/jcis.1999.6464.
[40] K. Xia, U.L. Skyllberg, W.F. Bleam, P.R. Bloom, E.A. Nater, P.A. Helmke, Environ. Sci. Technol. 33 (1999) 257.
[41] L. Pauling, J. Am. Chem. Soc. 51 (1929) 1010.
[42] I.D. Brown, R.D. Shannon, Acta Crystallogr. 29 (1973) 266.
[43] I.D. Brown, D. Altermatt, Acta Crystallogr. Sect. B 41 (1985) 244.
[44] N.E. Brese, M. Okeeffe, Acta Crystallogr. Sect. B 47 (1991) 192.
[45] F. Farges, C.W. Ponader, G.E. Brown Jr., Geochim. Cosmochim. Acta 55 (1991) 1563.
[46] F. Farges, C.W. Ponader, G. Calas, G.E. Brown Jr., Geochim. Cosmochim. Acta 56 (1992) 4205.
[47] J.R. Bargar, G.E. Brown Jr., G.A. Parks, Geochim. Cosmochim. Acta 61 (1997) 2617.
[48] J.R. Bargar, G.E. Brown Jr., G.A. Parks, Geochim. Cosmochim. Acta 61 (1997) 2639.
[49] J.R. Bargar, S.N. Towle, G.E. Brown Jr., G.A. Parks, J. Colloid Interface Sci. 185 (1997) 473, doi:10.1006/jcis.1996.4574.
[50] T. Hiemstra, W.H. van Riemsdijk, J. Colloid Interface Sci. 179 (1996) 488, doi:10.1006/jcis.1996.0242.
[51] R. Rietra, T. Hiemstra, W.H. van Riemsdijk, J. Colloid Interface Sci. 240 (2001) 384, doi:10.1006/jcis.2001.7650.
[52] J.D. Ostergren, T.P. Trainor, J.R. Bargar, G.E. Brown Jr., G.A. Parks, J. Colloid Interface Sci. 225 (2000) 466, doi:10.1006/jcis.1999.6701.
[53] C.S. Kim, J.J. Rytuba, G.E. Brown Jr., J. Colloid Interface Sci. 270 (2004) 9, doi:10.1016/j.jcis.2003.07.029.
[54] R.J. Atkinson, A.M. Posner, J.P. Quirk, J. Inorg. Nucl. Chem. 30 (1968) 2371.
[55] S. Brunauer, P.H. Emmett, E. Teller, J. Am. Chem. Soc. 60 (1938) 309.
[56] T.H. Suchanek, P.J. Richerson, J.R. Flanders, D.C. Nelson, L.H. Mullen, L.L. Brister, J.C. Becker, Environ. Monit. Assess. 64 (2000) 299.
[57] G.A. Waychunas, G.E. Brown Jr., Adv. X-Ray Anal. 37 (1994) 607.
[58] G.N. George, I.J. Pickering, EXAFSPAK, a Suite of Computer Programs for the Analysis of X-Ray Absorption Spectra, Stanford Synchrotron Radiation Laboratory, 1995.
[59] S.I. Zabinsky, J.J. Rehr, A. Ankudinov, R.C. Albers, M.J. Eller, Phys. Rev. B Condens. Matter Mater. Phys. 52 (1995) 2995.
[60] A.R. Davis, D.E. Irish, Inorg. Chem. 7 (1968) 1699.
[61] R.P.J. Cooney, J.R. Hall, Aust. J. Chem. 22 (1969) 337.
[62] R.P.J. Cooney, J.R. Hall, J. Inorg. Nucl. Chem. 34 (1972) 1519.
[63] H. Stammreich, T.T. Sans, J. Mol. Struct. 1 (1967) 55.
[64] A. Szytula, A. Burewica, Z. Dimitrijevic, S. Krasnicki, H. Rzany, J. Todorovic, A. Wanic, W. Wolski, Phys. Status Solidi 26 (1968) 429.
[65] N. Ishizawa, T. Miyata, I. Minato, F. Marumo, S. Iwai, Acta Crystallogr. Sect. B 36 (1980) 228.
[66] F. Zigan, W. Joswig, N. Burger, Z. Kristallogr. 148 (1978) 255.
[67] P. Avotins, Adsorption and Coprecipitation Studies of Mercury on Hydrous Iron Oxide, Ph.D. dissertation, Department of Civil Engineering, Stanford University, 1975.
[68] E.A. Forbes, A.M. Posner, J.P. Quirk, J. Colloid Interface Sci. 49 (1974) 403.
[69] P.G. Weidler, S.J. Hug, T.P. Wetche, T. Hiemstra, Geochim. Cosmochim. Acta 62 (1998) 3407.
[70] P.G. Weidler, T. Schwinn, H.E. Gaub, Clays Clay Miner. 44 (1996) 437.
[71] G. Sposito, The Surface Chemistry of Soils, Oxford Univ. Press, New York, 1984.
[72] C. Dyer, P.J. Hendra, W. Forsling, M. Ranheimer, Spectrochim. Acta A 49 (1993) 691.
[73] E. Laiti, P. Persson, L.O. Ohman, Langmuir 14 (1998) 825.
[74] H. Wijnja, C.P. Schulthess, Spectrochim. Acta A 55 (1999) 861.
[75] K. Aurivillius, Acta Crystallogr. 9 (1956) 685.
[76] S.N. Towle, J.R. Bargar, G.E. Brown Jr., G.A. Parks, J. Colloid Interface Sci. 187 (1997) 62, doi:10.1006/jcis.1996.4539.
[77] A.M. Scheidegger, G.M. Lamble, D.L. Sparks, J. Colloid Interface Sci. 186 (1997) 118, doi:10.1006/jcis.1996.4624.

[78] H.A. Thompson, G.A. Parks, G.E. Brown Jr., Geochim. Cosmochim. Acta 63 (1999) 1767.
[79] T.P. Trainor, G.E. Brown Jr., G.A. Parks, J. Colloid Interface Sci. 231 (2000) 359.
[80] C.J. Chisholm-Brause, K.F. Hayes, A.L. Roe, G.E. Brown Jr., G.A. Parks, J.O. Leckie, Geochim. Cosmochim. Acta 54 (1990) 1897.
[81] J.P. Fitts, G.E. Brown Jr., G.A. Parks, Environ. Sci. Technol. 34 (2000) 5122.
[82] D. Grdenic, G. Tunell, in: K.H. Wedepohl (Ed.), Mercury: Crystal Chemistry, Springer-Verlag, New York, 1969, p. 8.
[83] N.V. Pervukhina, G.V. Romanenko, S.V. Borisov, S.A. Magarill, N.A. Palchik, J. Struct. Chem. 40 (1999) 461.
[84] W. Forsling, S. Hietanen, L.G. Sillen, Acta Chem. Scand. 6 (1952) 901.
[85] S. Fujita, H. Horii, T. Mori, S. Taniguchi, J. Phys. Chem. 79 (1975) 960.
[86] G.P. Halada, C.R. Clayton, J. Electrochem. Soc. 138 (1991) 2921.
[87] F. Champloy, K. Gruber, G. Jogl, C. Kratky, J. Synchrotron Radiat. 7 (2000) 267.
[88] M. Galeotti, B. Cortigiani, U. Bardi, B.V. Andryushechkin, A.N. Klimov, K.N. El'tsov, J. Electron Spectrosc. Relat. Phenom. 76 (1995) 91.
[89] L.X. Chen, P.L. Lee, D. Gosztola, W.A. Svec, M.R. Wasielewski, J. Synchrotron Radiat. 6 (1999) 403.
[90] R.S. Zhou, R.L. Snyder, Act. Crystallogr. Sect. B 47 (1991) 617.
[91] I. Olovsson, P. Jonsson, in: P. Schuster (Ed.), X-Ray and Neutron Diffraction Studies of Hydrogen Bonded Systems, North-Holland, New York, 1976, p. 394.
[92] T.H. Suchanek, P.J. Richerson, L.J. Mullen, L.L. Brister, J.C. Becker, A. Maxson, D.G. Slotton, The Role of the Sulphur Bank Mercury Mine Site (and Associated Hydrogeological Processes) in the Dynamics of Mercury Transport and Bioaccumulation Within the Clear Lake Aquatic Ecosystem, A Report Prepared for the USEPA, Region IX Superfund Program, UC Davis, 1997.